Research Article

Nano Research
2023, 16(2): 2798–2807

ISSN 1998-0124 CN 11-5974/O4
https://doi.org/10.1007/s12274-022-4936-8

# Natural biopolymers derived hydrogels with injectable, self-healing, and tissue adhesive abilities for wound healing

Bin Kong[1,2], Rui Liu[1], Yi Cheng[1], Xiaodong Cai[2], Junying Liu[2], Dagan Zhang[1] (✉), Hui Tan[2] (✉), and Yuanjin Zhao[1,3] (✉)

[1] *Department of Rheumatology and Immunology, The Affiliated Drum Tower Hospital of Nanjing University Medical School, Nanjing 210002, China*
[2] *Respiratory department, Shenzhen Children's Hospital, Shenzhen 518038, China*
[3] *Oujiang Laboratory (Zhejiang Lab for Regenerative Medicine, Vision and Brain Health), Wenzhou Institute, University of Chinese Academy of Sciences, Wenzhou 325001, China*



**Received:** 23 June 2022 / **Revised:** 15 August 2022 / **Accepted:** 18 August 2022

## ABSTRACT

Developing a biocompatible and multifunctional adhesive hydrogel with injectability and self-healing ability for promoting wound healing is highly anticipated in various clinical applications. In this paper, we present a novel natural biopolymer-derived hydrogel based on the aldehyde-modified oxidized guar gum (OGG) and the carboxymethyl chitosan (CMCS) for efficiently improving wound healing with the encapsulation of vascular endothelial growth factor (VEGF). As the hydrogels are synthesized via the dynamically reversible Schiff base linkages, it is imparted with excellent self-healing ability and good shear thinning behavior, which make the hydrogel be easily and conveniently injected through a needle. Besides, the physiochemical properties, including porous structure, mechanical strength and swelling ratio of the hydrogel can be well controlled by regulating the concentrations of the OGG. Moreover, the hydrogel can attain strong adhesion to the tissues at physiological temperature based on the Schiff base between the aldehyde group on the hydrogel and the amino group on the tissue. Based on these features, we have demonstrated that the VEGF encapsulated hydrogel can adhere tightly to the defect tissue and improve wound repair in the rat model of defected skin by promoting cell proliferation, angiogenesis, and collagen secretion. These results indicate that the multifunctional hydrogel is with great scientific significance and broad clinical application prospects.

## KEYWORDS

hydrogel, self-healing, injectability, tissue adhesive, wound healing

## 1 Introduction

Wounds occur frequently in our daily life, and the treatment of wounds has gradually evolved into a fundamental healthcare issue throughout the world in recent years [1, 2]. A variety of materials have been applied for wound repair, including natural biomaterials, such as chitosan (CS), collagen (COL), alginate, and synthetic biomaterials, such as polyvinyl alcohol, polycaprolactone, polyethylene glycol [3–6]. These biomaterials are usually in the form of hydrogels, electrospinning nanofibrous scaffolds, microfluidics microparticles, porous foams, and microneedle patches [7–10]. Among them, hydrogels are widely employed and have exhibited a verified value in wound healing since their intrinsic highly moisture and porous structures, which can be capable of absorbing tissue exudates, facilitate the penetration of oxygen and nutrients, maintain a moist condition in the wound area, as well as providing a biomimetic microenvironment of extracellular matrix to improve the proliferation of cells and repair of tissues [11, 12]. Although with many successes, most of the current hydrogels used in wound healing lack tissue adhesive ability, which cannot guarantee the long-term maintenance of the materials in the wound area. Besides, the biocompatibility of the adhesive hydrogels fabricated by synthetic materials is limited. Thus, developing a novel natural biopolymer-derived and multifunctional hydrogel adhesive for promoting wound healing is still highly anticipated.

In this paper, we present novel natural biopolymer-derived adhesive hydrogels fabricated by the Schiff base between the aldehyde modified oxidized guar gum (OGG) and the carboxymethyl chitosan (CMCS) for efficient wound healing, as shown in Fig. 1. To date, the formation of hydrogels has been reported via various covalent linkages, such as Michael addition, thio-ether, azide-alkyne cycloaddition, and Schiff base [13–15]. Among these linkages, the Schiff base has attracted great interest because of its intrinsic dynamic nature and pH-responsive behaviors, which can endow the hydrogel with self-healing and intelligently responsive properties [16–18]. Hyaluronic acid (HA) [17, 19–22], alginate [23–25], chondroitin sulfate [16, 26, 27], or polyethylene glycol [18, 28, 29] have been widely used after modification in the biomedical field to construct hydrogels with gelatin, gelatin methacrylate (GelMA), CMCS, or other materials with amins group based on Schiff base. Recently, guar gum (GG) has emerged and been exploited to study its potential value in tissue engineering and regenerative medicine. GG is derived from the seed of the plant Cyamopsis tetragonoloba, which is a natural heteropolysaccharide with high molecular weight. Due to its

Address correspondence to Dagan Zhang, zhang_dagan@126.com; Hui Tan, huitan@email.szu.edu.cn; Yuanjin Zhao, yjzhao@seu.edu.cn

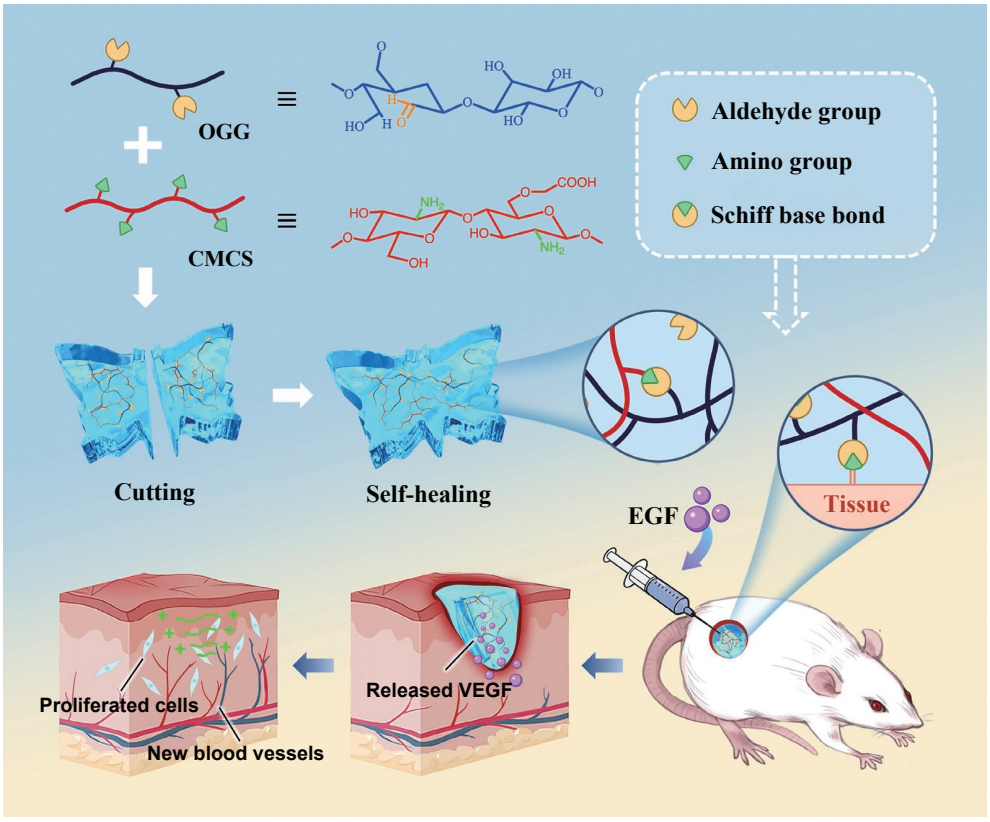


**Figure 1** Fabrication of the OGG/CMCS hydrogels with injectable, self-healing, and tissue adhesive abilities for wound healing.

biocompatible, sustainable, and biodegradable properties, GG has been extensively used as food thickening agent and in the drug delivery field [30]. In addition, there are adjacent hydroxyl groups on the molecular chain of GG, which allow it to be easily oxidized to incorporate aldehyde groups [31]. In contrast, CS is also a natural polysaccharide with biocompatible, antimicrobial and antioxidant properties, and has demonstrated its values in various applications [28, 32]. To overcome the poor water solubility, carboxymethyl chitosan has been synthesized. Although OGG and CMCS have been developed in their field, the physicochemical properties and wound healing capability of their composite hydrogel has not been investigated yet.

Herein, we constructed the desired OGG/CMCS composited hydrogels with injectable, self-healing, and tissue adhesive abilities, and demonstrated their values for efficiently improving wound healing with the encapsulation of vascular endothelial growth factors (VEGF). The hydrogels were formed through the dynamically reversible Schiff base linkages between the aldehyde group on the OGG and the amino group on the CMCS. The porous structure, mechanical strength, and swelling ratio of the hydrogel could be well controlled by regulating the concentrations of the OGG. It was found that the hydrogel exhibited excellent self-healing ability and the behavior of shear thinning, which made it easily and conveniently injected through a needle. In addition, the hydrogel could attain strong adhesion to the tissues at physiological temperature based on the Schiff base between the aldehyde group on the hydrogel and the amino group on the tissue. Based on these features, we have demonstrated that the VEGF encapsulated hydrogel can adhere tightly to the defect tissue and improve the wound repair in the rat model of defected skin by promoting cell proliferation through upregulating the expression of Ki67, reducing inflammatory response by inhibiting the expression of TNF-α, and enhancing angiogenesis and collagen secretion. Thus, we believe that the multifunctional hydrogel would supply the great scientific significance and broad clinical application prospects.

## 2 Experimental

### 2.1 Materials

All chemical materials not mentioned were purchased from Sigma-Aldrich (USA). The porcine skin used was bought from the local farmer's market. NIH-3T3 cells were provided by the Chinese Academy of Sciences. The cell culture-related materials, including Dulbecco's modified Eagle's medium (DMEM), fetal bovine serum (FBS), penicillin-streptomycin (PS), and trypsin were bought from Gibco (USA). The cell live-dead assay kit and cell counting kit-8 (CCK-8) were purchased from KeyGen Biotech corporation (Jiangsu, China). The primary antibody of Ki67, tumor necrosis factor-α (TNF-α), collagen, vimentin (VIM), α-smooth muscle actin (α-SMA) and CD 31, and the secondary antibody of Alexa Fluor 488 goat anti-rabbit immunoglobulin G (IgG), H&L, Alexa Fluor 594 goat anti-mouse IgG H&L, and horseradish peroxidase (HRP)-conjugated goat anti-rabbit IgG H&L were bought from Abcam (USA). The 6 weeks male Sprague–Dawley (SD) rat was bought from the Model Animal Research Center of Nanjing University.

### 2.2 Synthesis and characterization of OGG

The OGG was synthesized based on the previously reported method with a modification [31]. In brief, 1 g GG was firstly dissolved in 100 mL distilled water ($dH_2O$) under magnetic stirring at 90 °C for 1 h. Then, 250 mg $NaIO_4$ dissolved in 10 mL $dH_2O$ was added into the GG solution dropwise. After reacting for 24 h without light under vigorously stirring, 3 mL ethylene glycol was added to stop oxidation. Finally, the solution was dialyzed in $dH_2O$ for 5 days and freeze-dried for 3 days to obtain the OGG. An H nuclear magnetic resonance (HNMR) spectrometer (Bruker Avance NEO 600) and Fourier transform infrared (FTIR) spectrometer (Thermofisher, IN10) were used to obtain spectra to determine the chemical functional groups of the OGG.

### 2.3 Synthesis and characterization of CMCS

The CSCM was synthesized according to our previously reported method [29]. 1 g CS was firstly dissolved in 10 mL of isopropyl alcohol under magnetic stirring at room temperature (RT). Then, 5 mL sodium hydroxide solution (10 mol/L) was added to the CS solution dropwise. After stirring for 30 min, 10 mL monochloroacetic acid was added into five equal portions and stirred for 3 h. 10% hydrochloric acid solution was used to adjust the pH of the reaction mixture to about 7.4, followed by washing with methanol and alcohol. Finally, the solution was freeze-dried for 3 days to obtain the CMCS. An HNMR spectrometer (Bruker Avance NEO 600) and FTIR spectrometer (Thermofisher, IN10) were used to obtain spectra to determine the chemical functional groups of the CMCS.

### 2.4 Fabrication and characterization of the OGG/CMCS hydrogel

The OGG/CMCS hydrogel was fabricated by simply mixing the solution of OGG and CMCS. The same volume of OGG solution with the concentrations of 1%, 1.5%, and 2% was mixed with the CMCS solution with the concentrations of 3% and 6% to make the OGG/CMCS hydrogels with the final concentrations of OGG 0.5%, 0.75%, and 1%, CMCS 1.5% and 3%, respectively. The gelation time for the hydrogels with these different formulations was determined. The microscopic morphology of the hydrogels with the final concentrations of OGG 0.5%, 0.75%, and 1%, CMCS 1.5% were observed by scanning electron microscopy (SEM). All samples were frozen quickly in the liquid nitrogen and dried in a lyophilized, followed by the coating of a 20-nm-thick layer of gold. The morphology of these freeze-dried samples was imaged using an SEM (ZEISS, Germany). The pore size of the samples was measured using the software of Image J.

For the measurement of viscoelastic properties, a hybrid rheometer (Discovery HR-1, USA) was used. The hydrogels with a diameter of 10 mm and a height of 2 mm were prepared to match the clamp of the rheometer. The oscillatory frequency sweep for all samples was carried out at a fixed constant strain of 1% with a frequency ranging from 0.1 to 400 Hz, while the oscillatory strain sweep for all samples was performed at a constant frequency of 1 Hz. The oscillatory strain transformed from 1% for the interval of 80 s to 400% for the interval of 60 s, and a total of five cycles of transformation were performed for the continuous step strain measurement.

To measure the compressive mechanical properties, cylindrical hydrogels with a diameter of 10 mm and thickness of 5 mm were prepared. The compressive strain–stress curves and maximum compressive strength were recorded by using the mechanical testing machine.

For the measurement of swelling ratio, the cylindrical hydrogels with a diameter of 5 mm and height of 3 mm were prepared. The hydrogels were immersed in phosphate buffered saline (PBS) for 1, 2, 3, 4, 5, 6, 7, 8, 10, 12, 16, 20, and 24 h, respectively. The wet weight of the samples at each time point was measured after wiping off the redundant water with Kimwipe paper. Then, the samples were frozen quickly in the liquid nitrogen and dried in a lyophilizer, followed by the measurement of the dry weight. The swelling ratios were determined by dividing the dry weight by the wet weight of the samples. Three samples were measured for each condition to assure the reliability of the data.

The wound closure test and shear strength of the hydrogels with different formulations on the porcine skin were measured, respectively, by using a mechanical testing machine. For the wound closure test, the rectangular porcine skin with a width of 10 mm and thickness of 1 mm was prepared. The hydrogels were formed *in situ* between two skins with an area of 10 mm × 1 mm. The adhesion strength for the wound closure test was calculated by the following equation: adhesion strength = $F_{max}$/adhesion area, where $F_{max}$ is the maximum force. For the measurement of shear strength, the rectangular porcine skin with a width of 10 mm and length of 40 mm was prepared. The sealants were added between two tissues with an adhesion area of 15 mm by 10 mm. The shear strength was calculated by the following formula: shear strength = $F_{max}$/adhesion area, where $F_{max}$ is the maximum force. Three samples were measured for each condition to assure the reliability of the data.

### 2.5 *In vitro* biocompatibility evaluation

The extracts of the OGG/CMCS hydrogel with the final concentrations of OGG 1%, CMCS 1.5% were prepared by immersing a certain amount of the hydrogel into the culture media for 24 h at 37 °C. The 3T3 cells were cultured in the extracts with different concentrations (5, 10, and 15 mg/mL) after culturing for 24, 48, and 72 h, and the cells cultured under normal culture media were used as control. At each time point, a live/dead assay was performed by staining the cells with the mixture of ethidium homodimer and Calcein-AM solution, followed by the observation by a fluorescent microscope (Leica, Germany). The cell counting kit-8 was utilized to determine cell viability. In brief, the cells were incubated in the mixture of CCK-8 solution and culture media in the dark for 2 h at 37 °C, followed by the measurement of the optical density (OD) at 450 nm by using a plate reader. Three samples were measured for each condition to assure the reliability of the data.

### 2.6 *In vitro* vascularization evaluation

In order to evaluate the bioactivity of VEGF incorporated in the OGG/CMCS hydrogel, wound healing assay and tube formation experiments of human umbilical vein endothelial cells (HUVECs) were performed. The VEGF incorporated hydrogel was put in the incubator at 37 °C for 7 days, followed by the immersion in the HUVECs culture medium for 24 h to obtain the extracted liquid. For wound healing assay, $2 \times 10^5$ HUVECs were seed in 12-well plate. After culturing for 24 h, the cell layer was scratched with a 10 μL pipette tip to obtain the wound. The culture medium was removed, followed by the addition of the extracted liquid, and fresh culture medium with VEGF, respectively. In the control group, the fresh culture medium without VEGF was added. HUVECs were further cultured and photographed at 0, 24, and 48 h. Image J was used to analyze the degree of wound healing. Tube formation was evaluated by culturing the starvation-treated HUVECs in a 96-well plate coated with Matrigel. The culture medium was removed, followed by the addition of the extracted liquid, and fresh culture medium with VEGF, respectively. In the control group, the fresh culture medium without VEGF was added. After incubating for 6 h, the formed capillary-like structures were stained with Calcein-AM and observed using fluorescent microscopy (Leica, Germany). Image J was used to analyze the numbers of junctions, meshes, and total tube length.

### 2.7 Animal models

The animals were maintained in a temperature-controlled environment (20 ± 1 °C) with free access to food and water. Animal care, breeding, and euthanasia were performed with the approval of the Animal Ethics Committee of Nanjing University. The fifteen male SD rats of 6-week-old were divided into five groups evenly. One group was used to determine the *in vivo* biocompatibility of the materials, in which the hydrogel was performed subcutaneous implant to the rat, respectively for 2

weeks, followed by the harvest of main tissues, including heart, liver, spleen, lung, and kidney for further evaluation. The other four groups were used to perform the wound healing experiments. A defect with a diameter of 10 mm was generated on the skin of the rats by using a surgical trephine, and PBS, VEGF, OGG/CMCS hydrogel, and OGG/CMCS hydrogel incorporated with VEGF were added into the defected area, respectively. The defected area without treatment was used as a control group. All surgeries were carried out in sterile environments. Immediately, 3, 5, and 7 days after the operation, the defected area was observed and photographed by a digital camera, followed by the sacrifice of the rats to obtain the tissues around the defected area for further evaluation.

### 2.8 Histology, immunohistochemistry, and immunofluorescence Staining

All tissues obtained were fixed in 4% formaldehyde and then dehydrated in a series of gradient ethanol before vitrification by dimethylbenzene. The treated tissues were embedded in paraffin and sliced into slides with a thickness of 5 μm by a microtome. For Hematoxylin and Eosin (HE) and MASSON staining, the slices were deparaffinized, rehydrated, and then immersed into the specific staining solutions according to the manufacturer's manual, respectively. For immunohistochemistry analysis, the slices were deparaffinized, rehydrated, and then incubated with primary antibodies (Ki67 and TNF-α) and secondary antibodies, followed by the staining with 3,3'-diaminobenzidine (DAB) and hematoxylin. For immunofluorescence staining, the slides were deparaffinized, rehydrated, and then incubated with primary antibodies (collagen, vimentin, CD 31, and α-SMA) and secondary antibodies, followed by the mounting with 4,6-diamidino-2-phenylindole (DAPI) solution. The slides were observed under fluorescent microscopy (Leica, Germany).

### 2.9 Statistical analysis

All the results are presented as the means ± standard deviation. Statistical analysis was carried out using *t*-tests to determine the degree of significance. Statistical significance was defined as $*p < 0.05$, $**p < 0.01$, and $***p < 0.001$.

## 3 Results and discussion

In a typical experiment, the OGG was synthesized via the oxidation of GG with sodium meta periodate ($NaIO_4$) (Fig. S1(a) in the Electronic Supplementary Material (ESM)). The $^1$H nuclear magnetic resonance ($^1$HNMR) spectra shown in Fig. S1(b) in the ESM indicated a characterized peak at 9.3 ppm, which was attributed to the aldehydic proton. The FTIR spectrum (Fig. S1(c) in the ESM) showed the appearance of two characteristic peaks at 886 and 1,727 $cm^{-1}$ on the OGG, which ascribed to the formation of hemiacetal bond and the aldehyde symmetrical vibration. The $^1$HNMR and FTIR results indicated that the OGG was successfully synthesized. Moreover, the oxidization degree of the OGG was about 67.8% measured by comparing with the standard curve (Fig. S2 in the ESM). To determine the synthesis of CMCS, the analysis of 1HNMR and FTIR of CS and CMCS was performed as well (Fig. S3 in the ESM). From Fig. S3(b) in the ESM, the peaks at 3.2–3.5 ppm indicated the H-2 proton of carboxymethyl. From Fig. S3(c) in the ESM, the FTIR spectrum of CMCS exhibited the presence of the bands at 1,415–1,400 and 1,598–1,651 $cm^{-1}$, which signified the appearance of carboxymethyl groups on the CMCS. The $^1$HNMR and FTIR results indicated that the CMCS was successfully synthesized.

The OGG/CMCS hydrogel was fabricated by simply mixing the OGG and CMCS solutions based on the dynamically reversible Schiff base linkages between the aldehyde group on the OGG and the amino group on the CMCS (Fig. S4(a) in the ESM). Although the same component of OGG and CMCS has been reported to construct the hydrogel previously [33], their work only focused on the physiochemical characterization and *in vitro* cell biocompatibility of the hydrogel. In our work, we investigated and demonstrated for the first time the potential value of the OGG/CMCS hydrogel for wound healing and tissue regeneration, which has not been previously studied or reported. Gelation time is essential for hydrogels used in injectable applications. Rapid gelation might cause the formation of hydrogels before injection, while slow gelation might result in the diffusion of the solutions after injection before the gel formation [34, 35]. Therefore, we measured the gelation time of the OGG/CMCS hydrogel under different formulations. From Fig. S4(b) in the ESM, the final concentration of 3 wt.% CMSC rendered a faster gelation time compared with that of 1.5 wt.% due to the higher crosslinking density. And based on 3 wt.% CMSC, the gelation times of 1 wt.%, 0.75 wt.%, and 0.5 wt.% OGG were 17.7 ± 2.5, 44.3 ± 4, and 75.3 ± 5 s, respectively, which were suitable for *in vivo* injection, and the following experiments were all based on these formulations. The microscopic structures of the OGG/CMCS hydrogels were firstly determined via the SEM observation of the freeze-dried samples and fluorescent microscopy analysis of freshly prepared samples (Figs. 2(a)–2(f) and Fig. S5 in the ESM). It was noticed that the formulations could affect the porous structure of the hydrogel and the OGG/CMCS-1% hydrogel displayed relatively smaller pore sizes and tighter network structures compared with the OGG/CMCS-0.75% and OGG/CMCS-0.5% (Fig. S6 in the ESM).

In addition, good homogeneity has been discovered that can facilitate the enhancement of the mechanical strength of the hydrogel, meanwhile supplying a more appropriate environment for cells to adhere and proliferate [36, 37]. Therefore, the dynamic rheology of OGG/CMCS hydrogels with different formulations was carried out. From Figs. 2(g) and 2(h), the storage modulus (*G*') of all hydrogels was larger than the loss modulus (*G*"), indicating the formation of the free-standing hydrogel. From the modulus–strain curves shown in Fig. 2(i), when the strain was lower than 100%, the modulus of all OGG/CMCS maintained constant, and *G*' was larger than *G*", indicating that all hydrogels had a stable network structure within this strain range. With the continuous increase of strain, *G*' of OGG/CMCS all decreased and ultimately lowered than *G*", suggesting that the network structure of the hydrogels has been destroyed. Meanwhile, the yielding modulus of OGG/CMCS-1% was the largest, followed by OGG/CMCS-0.75%, and OGG/CMCS-0.5% was the smallest, indicating the mechanical property of OGG/CMCS hydrogel correlated nicely with its microstructures. Moreover, the compressive mechanical strength of the hydrogels was also measured, as shown in Figs. 2(j) and 2(k). The maximum compressive strength of the OGG/CMCS-1% was larger than OGG/CMCS-0.75%, and OGG/CMCS-0.5% was the smallest, which was consistent with the rheologic result. The swelling ability is a fundamental characteristic of the hydrogel, which can indicate the degree of hydrophilicity. Thus, the swelling ratio of OGG/CMCS hydrogel was further measured, as shown in Fig. 2(l). The swelling ratio of OGG/CMCS hydrogel reached 2.05 ± 0.15, 1.56 ± 0.15, and 1.12 ± 0.13 with the OGG concentration of 0.5%, 0.75%, and 1%, respectively, which was consistent with the SEM results of the hydrogel.

Injectable hydrogel with self-healing abilities has been widely used and demonstrated its values in the area of drug delivery and tissue regeneration [38, 39]. Therefore, we determined the shear thinning properties of OGG/CMCS hydrogel with different formulations. From Fig. 3(a), the viscosity of all hydrogels

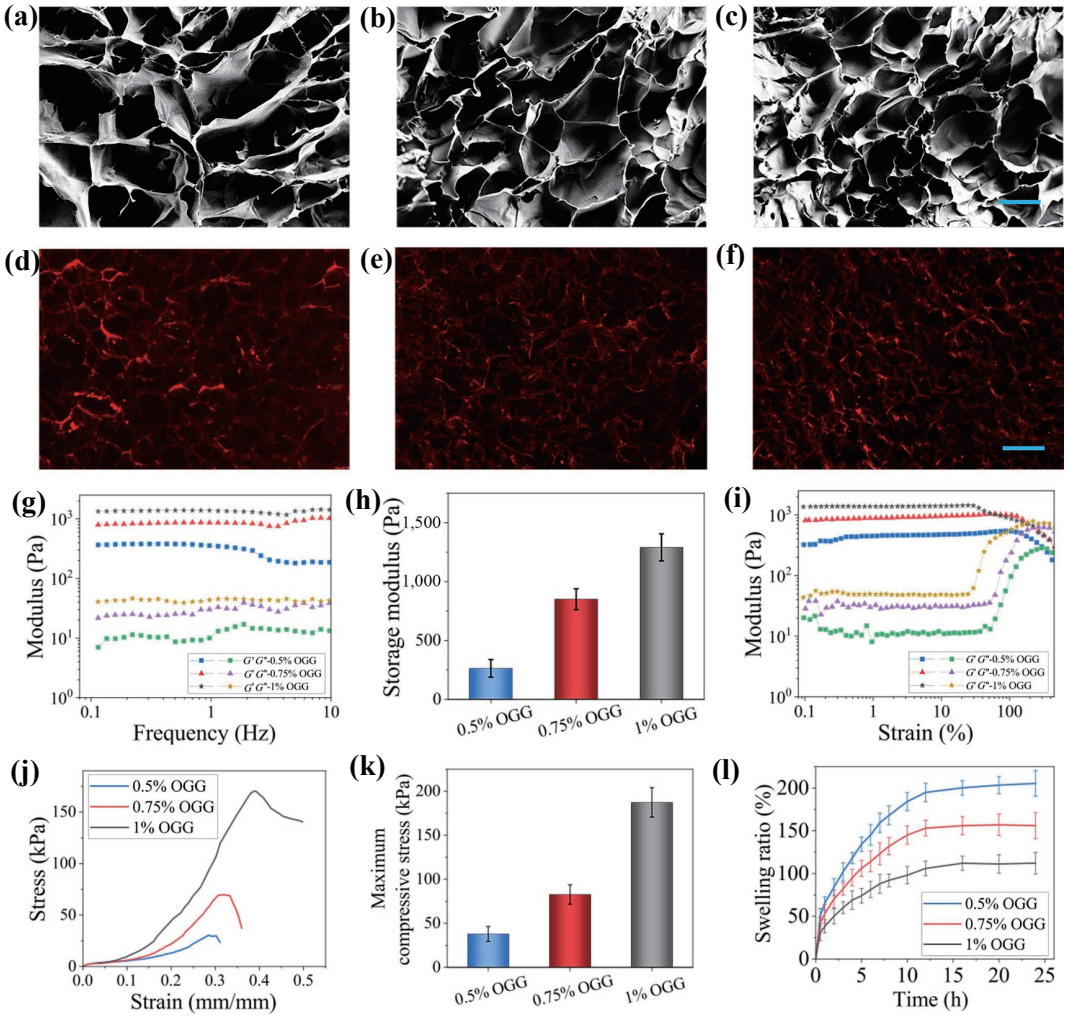


**Figure 2** Fabrication and characterization of the OGG/CMCS hydrogel. (a)–(c) SEM and ((d)–(f)) fluorescent images of OGG/CMCS hydrogels with the concentration of OGG 0.5%, 0.75%, and 1%, respectively. The scale bar in ((a)–(c)) was 20 μm, and in ((d)–(f)) was 50 μm. (g) Rheology analysis of OGG/CMCS hydrogels with different formulations on frequency sweeps. (h) The histogram of the storage modulus of OGG/CMCS hydrogels with different formulations on frequency sweeps. (i) Rheology analysis of OGG/CMCS hydrogels with different formulations on strain sweeps. (j) The compressive strain–stress curves of OGG/CMCS hydrogels with different formulations. (k) The histogram of the maximum compressive stress of OGG/CMCS hydrogels. (l) The swelling ratios of OGG/CMCS hydrogels with different formulations.

decreased with the increase of shear rates under 1% constant strain, indicating the great shear-thinning property, which endowed the hydrogel with excellent injectability. Besides, we used a syringe to load the OGG/CMCS hydrogels, which can be easily extruded out via 25-gauge needles without clogging (Figs. 3(b) and 3(c)). To verify the self-healing ability, two OGG/CMCS hydrogels with the shape of a butterfly and incorporated with yellow dye and blue dye, respectively, were prepared (Fig. 3(d)). The hydrogels were cut into two parts using a surgical blade, and one part of the hydrogel with yellow dye was contacted closely with that of the blue dye. After contacting for 2 h, the two parts were healed into one unit and could bear its weight and hang against gravity (Fig. 3(e)). And the self-healed hydrogel could be stretched to nearly twice its initial length without any tearing at the joint (Fig. 3(f)). In addition, we determined the rheological self-healing behaviors of the OGG/CMCS hydrogels via continuous step strain measurement. The oscillatory strain transformed from 1% for the interval of 80 s to 400% for the interval of 60 s, and a total of five cycles of transformation were performed. From Fig. 3(g), when the strain was 400%, $G'$ was smaller than $G''$, suggesting that the hydrogel was broken. However, $G'$ was immediately restored to its original value when the strain switched to 1% and larger than $G''$. The results suggested the excellent self-healing ability of the OGG/CMCS hydrogel. Good biocompatibility and low immunogenicity were essential for the materials used in regenerative medicine [40, 41].

In addition to the excellent injectable and self-healing abilities, the OGG/CMCS hydrogels also exhibited adequate adhesion to the tissues. The OGG/CMCS hydrogel incorporated with the orange dye was formed *in situ* on the porcine skin and could adhere tightly to the skin without any detachment under stretch, distortion, bend or even immersing into water for 24 h, indicating that the OGG/CMCS hydrogel had quite strong tissue binding power (Fig. S7 in the ESM). We further compared the adhesiveness of OGG/CMCS with different formulations by using a wound closure test and lap-shear adhesion test. From Fig. 3(h), the OGG/CMCS-1% hydrogel exhibited an adhesion strength of 45 ± 1.6 kPa, which was higher than the OGG/CMCS-0.75% hydrogel (35 ± 1 kPa), and significantly higher than the OGG/CMCS-0.5% hydrogel (29 ± 0.7 kPa). In the lap-shear adhesion test, the OGG/CMCS-1% hydrogel exhibited a shear strength of 12 ± 1.6 kPa, which was higher than the OGG/CMCS-0.75% hydrogel (8 ± 0.4 kPa), and significantly higher than the OGG/CMCS-0.5% hydrogel (5 ± 0.7 kPa) (Fig. 3(i)).

To verify the biocompatibility of OGG/CMCS hydrogel, the extracted liquid of the hydrogel with concentrations of 5, 10, and 15 mg/mL was used to culture NIH-3T3 cells. The 3T3 cells were cultured in the plastic culture dish under normal culture media (control) and extract liquid of the patch with three concentrations

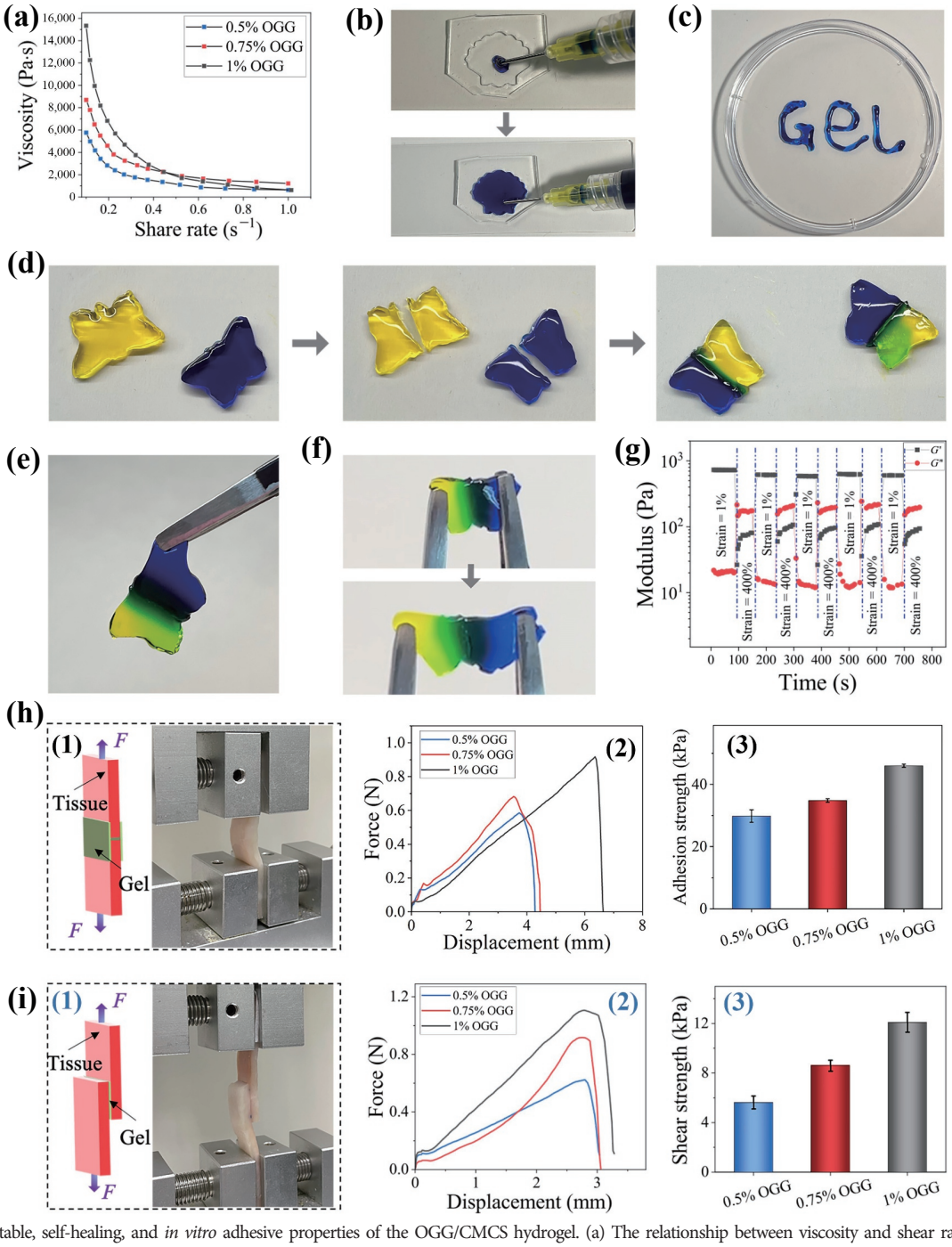


**Figure 3** Injectable, self-healing, and *in vitro* adhesive properties of the OGG/CMCS hydrogel. (a) The relationship between viscosity and shear rate. (b)–(c) The injectability and extrudability of the hydrogel. (d)–(f) The self-repaired hydrogel and displaying stretchability. (g) Continuous step-strain measurements were applied to the hydrogel in step of 1% and 400% oscillatory strain for cycles. (h) and (i) Measurement of wound closure strength and shear strength of OGG/CMCS hydrogels with different formulations: (1) schematic illustration and photography showing the adhesion of OGG/CMCS hydrogels on porcine skin for tests, (2) the force–displacement curves, and (3) histogram of the adhesion strength and shear strength of ((b) and (c)).

(cell-h) for 24, 48, and 72 h, respectively. From the live/dead staining and CCK8 assay results, as shown in Figs. 4(a) and 4(b), and Fig. S8 in the ESM. At 24 h, the viability of cell-h was higher than the control, indicating that the hydrogel can promote the proliferation of cells, which is attributed to the component of the hydrogel. As GG is a natural heteropolysaccharide and chitosan is also a natural polysaccharide, the extracted liquid of the hydrogel can provide additional nutrients for the cells to promote cell proliferation. With the extension of culture time, the extra nutrients will be gradually consumed by the cells. As a result, the proliferation of cell-h will gradually decrease, and the cell viability will decrease accordingly. Although the appearance of decrease, the viability of cell-h maintains at a higher level than that of the control during all culture times, indicating that the hydrogel has good biocompatibility. In order to evaluate the bioactivity of VEGF incorporated in the OGG/CMCS hydrogel, wound healing assay and tube formation experiments of HUVECs were performed. From Figs. 4(c)–4(f), vessel formation capacities of HUVECs treated with VEGF and VEGF loaded hydrogel were significantly elevated in comparison to the untreated cells in the control group, and the VEGF loaded hydrogel exhibited better vessel formation capacities than the VEGF group. From Fig. 4(g) and Fig. S9 in the ESM, the VEGF could significantly promote the closure of scratches in VEGF group and VEGF loaded hydrogel group compared to the untreated HUVECs group. The results indicated that VEGF could maintain long-term activity in our

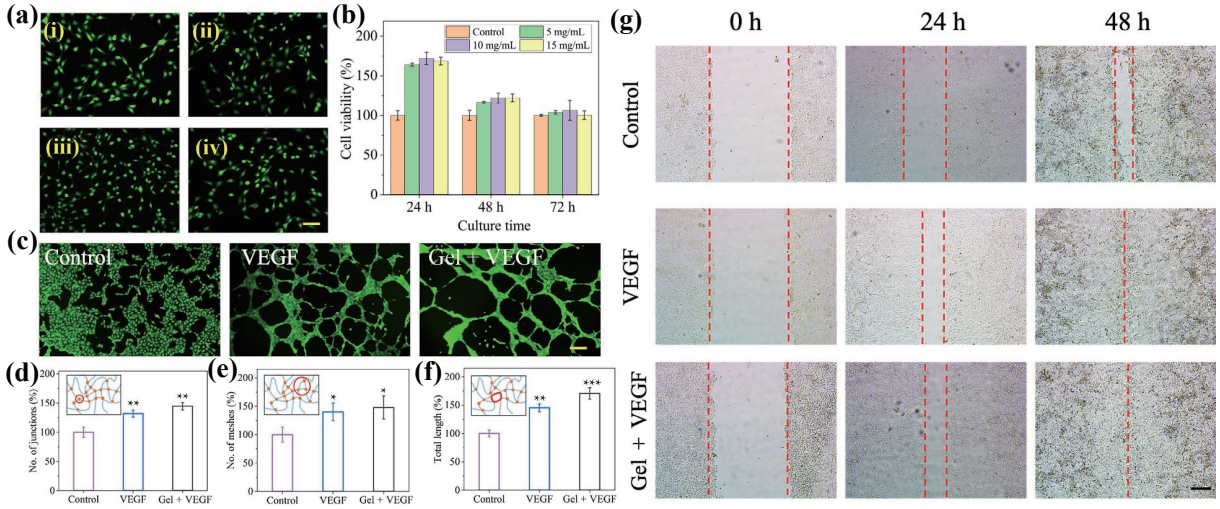


**Figure 4** Biocompatibility characterization and biological activity of VEGF in OGG/CMCS hydrogel. (a) The live/dead staining images of 3T3 cells after culturing in the extracted liquid of the hybrid patch with the concentrations of (i) 0, (ii) 5, (iii), 10 and (iv)15 mg/mL for 24 h. (b) The cell viability in the extracted liquid after culturing for 24, 48, and 72 h. (c) Images and ((d)–(f)) quantitative analysis of tube formation with various treatments in HUVECs. (g) Images of wound healing assay with various treatments in HUVECs. The scale bar is 100 μm.

hydrogel.

After the characterization and evaluation of the OGG/CMCS hydrogel *in vitro*, we then verified their performance *in vivo* in the rat model of defected skin. The OGG/CMCS hydrogel was firstly embedded into the subcutaneous area of the rats for 14 days to assess the long-term *in vivo* biocompatibility, and the normal rats were as the control. The main tissues, including the heart, liver, spleen, lung, and kidney, were stained with HE. As shown in Fig. S10 in the ESM, the main tissues were not influenced by the implantation of the hydrogel when compared with the tissues of the normal rats. The OGG/CMCS hydrogel incorporated with VEGF, pure OGG/CMCS hydrogel, and VEGF and PBS were added into the defected area, and the group without treatment was as control. The defected area in all groups was photographed at 0, 3, 5, and 7 days (Fig. 5(a)). As we know, angiogenesis plays an essential role during the process of wound healing since it not only provides the oxygen and nutrients required by the regenerated tissues, but also promotes the structural repair via the formation of granulation tissues. VEGF has been demonstrated as a crucial factor in angiogenesis. It can promote the endothelial cells to permeate, grow and migrate. Besides, VEGF can facilitate the epithelialization and deposition of collagen compared to other angiogenic growth factors, such as b-FGF and TGF-β. In addition, the hydrogels could also provide structural support for the formation of new granulation tissue and blood vessels. Thus, the wound closure rate in the wound bed was significantly higher in the VEGF incorporated hydrogel-treated rats than in the groups. (Fig. 5(c)). On day 7, the defected tissues were harvested and firstly performed with HE staining, and the thickness of the granulation tissue was determined. From Figs. 5(b) and 5(d), the thickness of the granulation tissue in the OGG/CMCS hydrogels and VEGF treated rats was both higher than the PBS group and control group. Notably, the wound repair performance was enhanced by adding the VEGF (Figs. 5(b)–5(d)). Besides, the cell proliferation and local inflammatory response of the defected area were visualized via immunohistochemical staining of Ki67 and TNF-α (Figs. 5(e) and 5(f) and Fig. S11 in the ESM). The Ki67-positive cells of the hydrogel groups were significantly larger than the PBS and control groups (Fig. S12(a) in the ESM). Large inflammatory cells were infiltrated and observed in all groups, in contrast, and the inflammatory cells in the hydrogel groups were significantly lower than the other groups (Fig. S12 (b) in the ESM).

To further verify the wound repairing ability of the OGG/CMCS hydrogel, MASSON staining was performed. From Fig. 6(a), the collagen was present and the amount of the secreted collagen in the hydrogel groups was significantly larger than in the other groups (Fig. 6(d)). In addition, the double immunofluorescent staining of collagen and vimentin was carried out to determine the deposition of collagen as well. VIM was specifically expressed in the fibroblast and Fig. 6(b) suggested that the collagen fibers were predominantly spread around the fibroblasts, indicating the collagen production ability of these fibroblasts. And more deposition and higher alignment degree of collagen fibers in the hydrogel groups were observed than in the other groups. The influence of four treatments on the neovascularization of the defected area was evaluated via immunofluorescence staining against CD31 and α-SMA, which were specifically expressed in endothelial cells and smooth muscle cells, respectively, and markers for angiogenesis. From Figs. 6(c) and 6(e), the number of blood vessels was significantly improved in the VEGF incorporated hydrogel groups. The results suggested the OGG/CMCS hydrogel is an ideal scaffold for remodeling and repairing different wounds.

## 4 Conclusions

In summary, we constructed a natural biopolymer-derived hydrogels OGG/CMCS with injectable, self-healing, and tissue adhesive abilities to efficiently improve wound healing with the encapsulation of VEGF. The hydrogel is formed through the dynamically reversible Schiff base linkages between the aldehyde group on the OGG and the amino group on the CMCS. The porous structure, mechanical strength, and swelling ratio of the hydrogel can be well controlled by regulating the concentrations of the OGG. Besides, the hydrogel exhibited excellent self-healing ability and the behavior of shear thinning, which make it easily and conveniently injected through a needle. Moreover, the hydrogel can attain strong adhesion to the tissues at physiological temperature. We have demonstrated that the VEGF encapsulated hydrogel can adhere tightly to the defect tissue and improve wound repair in the rat model of defected skin by promoting cell proliferation through upregulating the expression of Ki67, reducing inflammatory response by inhibiting the expression of TNF-α, and enhancing angiogenesis and collagen secretion. Thus, we believe that the multifunctional hydrogel would supply the great scientific significance and broad clinical application

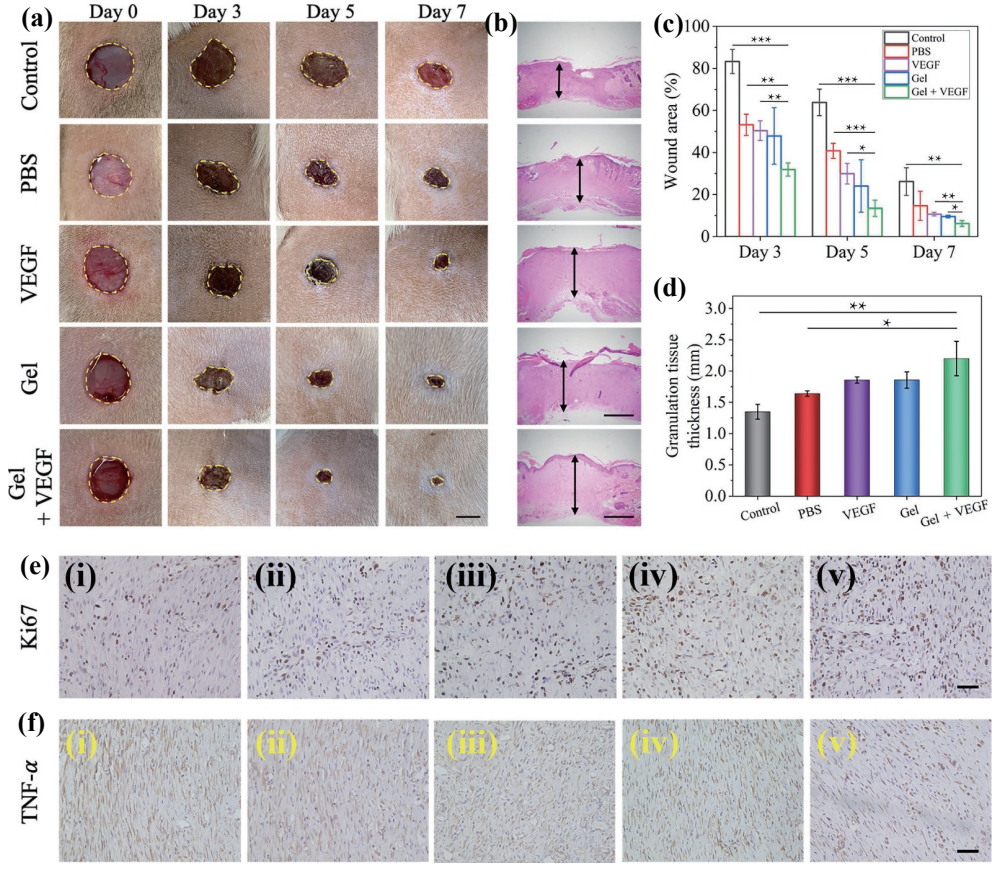


**Figure 5** The evaluation of the OGG/CMCS hydrogel *in vivo*. (a) Photographs showing the defected wounds on day 0, 3, 5, and 7. The scale bar is 5 mm. (b) HE staining of the defected area 7 days after the operation. The scale bar is 1 mm. (c) The area of the defected area. (d) Histogram showing the thickness of the defected tissue. (e) and (f) Immunostaining of Ki67 and TNF-α in the defected tissue at day 7 under high magnification. The scale bar is 50 μm.

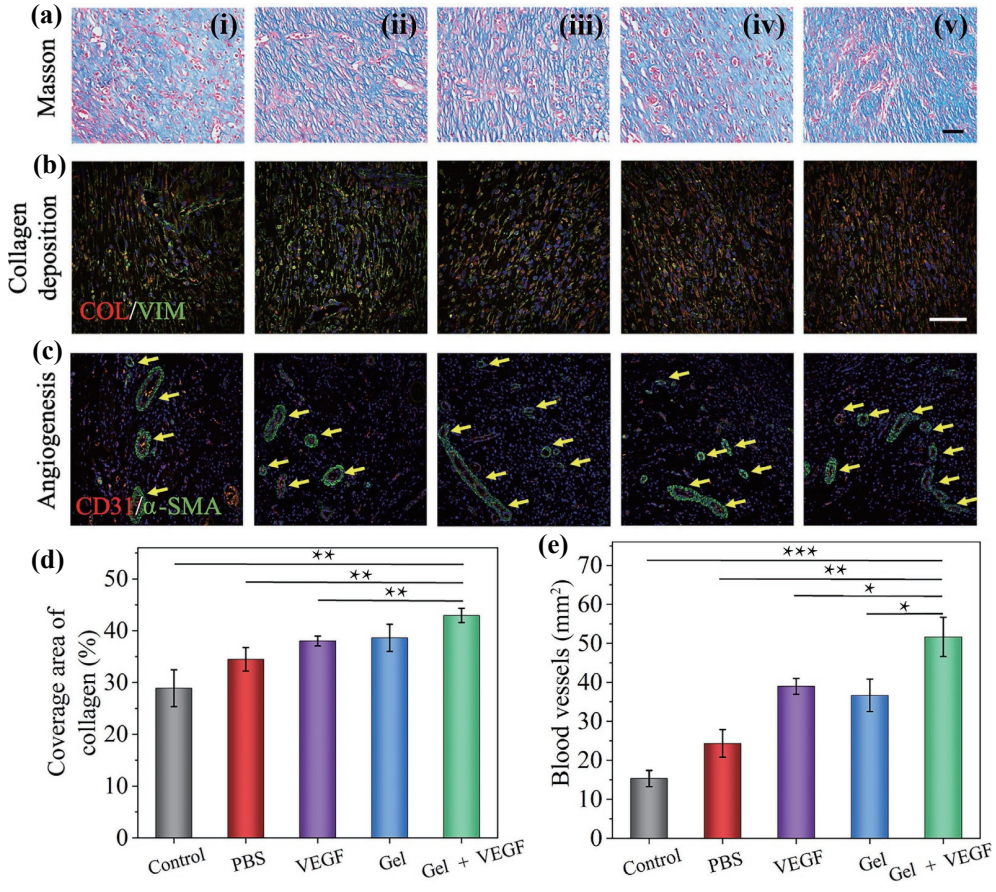


**Figure 6** The wound healing of the OGG/CMCS hydrogel *in vivo*. (a) Masson staining of the defected area 7 days after the operation. (b) Double immunofluorescent staining of collagen (green) and vimentin (red). (c) Double immunofluorescent staining of CD 31 (red) and α-SMA (green). The yellow arrows implied the vascular ducts. The scale bar in ((a)–(b)) is 50 μm, and in (c) is 100 μm. (d)–(e) Quantification of collagen and CD31 labeled blood vessels.

prospects.

## Acknowledgements

This work was supported by the National Natural Science Foundation of China (Nos. 82101184 and 82102511), the Shenzhen Fundamental Research Program (Nos. JCYJ20210324102809024, JCYJ20190813152616459 and JCYJ20210324133214038), the Shenzhen PhD Start-up Program (Nos. RCBS20210609103713045, ZDSYS20200811142600003, JCYJ20180228162928828, and JCYJ20190806161409092), the Natural Science Foundation of Guangdong Province (No. 2020A1515110780), the Guangdong Basic and Applied Basic Research Foundation (No. 2021B1515120054), the Natural Science Foundation of Jiangsu (No. BK20210021), and the Research Project of Jiangsu Province Health Committee (No. M2021031).

**Electronic Supplementary Material:** Supplementary material (further details of the $^1$HNMR and FTIR spectrum measurements, the gelation and diameter range of the OGG/CMCS hydrogel, the *in-situ* adhesion of OGG/CMCS hydrogel on the porcine skins, the live/dead staining images for 48 and 72 h, the quantitative analysis of wound healing assay, HE staining of heart, liver, spleen, lung and kidney, and the quantification of Ki67 and TNF-α positive cells) is available in the online version of this article at https://doi.org/10.1007/s12274-022-4936-8.

## References

[1] Chen, H. H.; Cheng, Y. H.; Tian, J. R.; Yang, P. Z.; Zhang, X. R.; Chen, Y. H.; Hu, Y. Q.; Wu, J. H. Dissolved oxygen from microalgae-gel patch promotes chronic wound healing in diabetes. *Sci. Adv.* **2020**, *6*, eaba4311.

[2] Blacklow, S. O.; Li, J.; Freedman, B. R.; Zeidi, M.; Chen, C.; Mooney, D. J. Bioinspired mechanically active adhesive dressings to accelerate wound closure. *Sci. Adv.* **2019**, *5*, eaaw3963.

[3] Zhang, J.; Zheng, Y. J.; Lee, J.; Hua, J. Y.; Li, S. L.; Panchamukhi, A.; Yue, J. P.; Gou, X. W.; Xia, Z. F.; Zhu, L. Y. et al. A pulsatile release platform based on photo-induced imine-crosslinking hydrogel promotes scarless wound healing. *Nat. Commun.* **2021**, *12*, 1670.

[4] Castaño, O.; Pérez-Amodio, S.; Navarro-Requena, C.; Mateos-Timoneda, M. Á.; Engel, E. Instructive microenvironments in skin wound healing: Biomaterials as signal releasing platforms. *Adv. Drug Deliv. Rev.* **2018**, *129*, 95–117.

[5] Mao, J. Y.; Chen, L.; Cai, Z. W.; Qian, S. T.; Liu, Z. M.; Zhao, B. F.; Zhang, Y. G.; Sun, X. M.; Cui, W. G. Advanced biomaterials for regulating polarization of macrophages in wound healing. *Adv. Funct. Mater.* **2022**, *32*, 2111003.

[6] Kong, B.; Sun, L. Y.; Liu, R.; Chen, Y.; Shang, Y. X.; Tan, H.; Zhao, Y. J.; Sun, L. Y. Recombinant human collagen hydrogels with hierarchically ordered microstructures for corneal stroma regeneration. *Chem. Eng. J.* **2022**, *428*, 131012.

[7] Chen, T. Y.; Wen, T. K.; Dai, N. T.; Hsu, S. H. Cryogel/hydrogel biomaterials and acupuncture combined to promote diabetic skin wound healing through immunomodulation. *Biomaterials* **2021**, *269*, 120608.

[8] Cui, C. J.; Sun, S. B.; Wu, S. H.; Chen, S. J.; Ma, J. W.; Zhou, F. Electrospun chitosan nanofibers for wound healing application. *Eng. Regener.* **2021**, *2*, 82–90.

[9] Liang, Y. P.; He, J. H.; Guo, B. L. Functional hydrogels as wound dressing to enhance wound healing. *ACS Nano* **2021**, *15*, 12687–12722.

[10] Yu, Y. R.; Chen, G. P.; Guo, J. H.; Liu, Y. X.; Ren, J. N.; Kong, T. T.; Zhao, Y. J. Vitamin metal-organic framework-laden microfibers from microfluidics for wound healing. *Mater. Horiz.* **2018**, *5*, 1137–1142.

[11] Liu, H.; Wang, C. Y.; Li, C.; Qin, Y. G.; Wang, Z. H.; Yang, F.; Li, Z. H.; Wang, J. C. A functional chitosan-based hydrogel as a wound dressing and drug delivery system in the treatment of wound healing. *RSC Adv.* **2018**, *8*, 7533–7549.

[12] Kong, B.; Chen, Y.; Liu, R.; Liu, X.; Liu, C. Y.; Shao, Z. W.; Xiong, L. M.; Liu, X. N.; Sun, W.; Mi, S. L. Fiber reinforced GelMA hydrogel to induce the regeneration of corneal stroma. *Nat. Commun.* **2020**, *11*, 1435.

[13] Sharma, P. K.; Singh, Y. Glyoxylic hydrazone linkage-based PEG hydrogels for covalent entrapment and controlled delivery of doxorubicin. *Biomacromolecules* **2019**, *20*, 2174–2184.

[14] Dong, R. N.; Zhao, X.; Guo, B. L.; Ma, P. X. Self-healing conductive injectable hydrogels with antibacterial activity as cell delivery carrier for cardiac cell therapy. *ACS Appl. Mater. Interfaces* **2016**, *8*, 17138–17150.

[15] Kharkar, P. M.; Kiick, K. L.; Kloxin, A. M. Designing degradable hydrogels for orthogonal control of cell microenvironments. *Chem. Soc. Rev.* **2013**, *42*, 7335–7372.

[16] Zhou, L.; Dai, C.; Fan, L.; Jiang, Y. H.; Liu, C.; Zhou, Z. N.; Guan, P. F.; Tian, Y.; Xing, J.; Li, X. J. et al. Injectable self-healing natural biopolymer-based hydrogel adhesive with thermoresponsive reversible adhesion for minimally invasive surgery. *Adv. Funct. Mater.* **2021**, *31*, 2007457.

[17] Hong, Y.; Zhou, F. F.; Hua, Y. J.; Zhang, X. Z.; Ni, C. Y.; Pan, D. H.; Zhang, Y. Q.; Jiang, D. M.; Yang, L.; Lin, Q. N. et al. A strongly adhesive hemostatic hydrogel for the repair of arterial and heart bleeds. *Nat. Commun.* **2019**, *10*, 2060.

[18] Chen, G. P.; Yu, Y. R.; Wu, X. W.; Wang, G. F.; Ren, J. N.; Zhao, Y. J. Bioinspired multifunctional hybrid hydrogel promotes wound healing. *Adv. Funct. Mater.* **2018**, *28*, 1801386.

[19] Chen, J. Q.; Yang, J. B.; Wang, L.; Zhang, X. W.; Heng, B. C.; Wang, D. A.; Ge, Z. G. Modified hyaluronic acid hydrogels with chemical groups that facilitate adhesion to host tissues enhance cartilage regeneration. *Bioact. Mater.* **2021**, *6*, 1689–1698.

[20] Wu, T. L.; Cui, C. Y.; Huang, Y. T.; Liu, Y.; Fan, C. C.; Han, X. X.; Yang, Y.; Xu, Z. Y.; Liu, B.; Fan, G. W. et al. Coadministration of an adhesive conductive hydrogel patch and an injectable hydrogel to treat myocardial infarction. *ACS Appl. Mater. Interfaces* **2019**, *12*, 2039–2048.

[21] Yang, B.; Song, J. L.; Jiang, Y. H.; Li, M.; Wei, J. J.; Qin, J. J.; Peng, W. J.; Lasaosa, F. L.; He, Y. Y.; Mao, H. L. et al. Injectable adhesive self-healing multicross-linked double-network hydrogel facilitates full-thickness skin wound healing. *ACS Appl. Mater. Interfaces* **2020**, *12*, 57782–57797.

[22] Pandit, A. H.; Mazumdar, N.; Ahmad, S. Periodate oxidized hyaluronic acid-based hydrogel scaffolds for tissue engineering applications. *Int. J. Biol. Macromol.* **2019**, *137*, 853–869.

[23] Lueckgen, A.; Garske, D. S.; Ellinghaus, A.; Desai, R. M.; Stafford, A. G.; Mooney, D. J.; Duda, G. N.; Cipitria, A. Hydrolytically-degradable click-crosslinked alginate hydrogels. *Biomaterials* **2018**, *181*, 189–198.

[24] Fan, C. Q.; Xu, K. G.; Huang, Y.; Liu, S.; Wang, T. C.; Wang, W.; Hu, W. C.; Liu, L.; Xing, M.; Yang, S. M. Viscosity and degradation controlled injectable hydrogel for esophageal endoscopic submucosal dissection. *Bioact. Mater.* **2021**, *6*, 1150–1162.

[25] Reakasame, S.; Boccaccini, A. R. Oxidized alginate-based hydrogels for tissue engineering applications: A review. *Biomacromolecules* **2018**, *19*, 3–21.

[26] Li, T.; Song, X. B.; Weng, C. M.; Wang, X.; Sun, L.; Gong, X. Y.; Yang, L.; Chen, C. Self-crosslinking and injectable chondroitin sulfate/pullulan hydrogel for cartilage tissue engineering. *Appl. Mater. Today* **2018**, *10*, 173–183.

[27] Zhou, L.; Fan, L.; Zhang, F. M.; Jiang, Y. H.; Cai, M.; Dai, C.; Luo, Y. A.; Tu, L. J.; Zhou, Z. N.; Li, X. J. et al. Hybrid gelatin/oxidized chondroitin sulfate hydrogels incorporating bioactive glass nanoparticles with enhanced mechanical properties, mineralization, and osteogenic differentiation. *Bioact. Mater.* **2021**, *6*, 890–904.

[28] Yin, X. Y.; Hao, Y. P.; Lu, Y.; Zhang, D. J.; Zhao, Y. D.; Mei, L.; Sui, K. Y.; Zhou, Q. H.; Hu, J. L. Bio-multifunctional hydrogel patches for repairing full-thickness abdominal wall defects. *Adv.*

*Funct. Mater.* **2021**, *31*, 2105614.
[29] Nie, M.; Kong, B.; Chen, G. P.; Xie, Y.; Zhao, Y. J.; Sun, L. Y. MSCs-laden injectable self-healing hydrogel for systemic sclerosis treatment. *Bioact. Mater.* **2022**, *17*, 369–378.
[30] Li, S. X.; Wang, L.; Zheng, W. F.; Yang, G.; Jiang, X. Y. Rapid fabrication of self‐healing, conductive, and injectable gel as dressings for healing wounds in stretchable parts of the body. *Adv. Funct. Mater.* **2020**, *30*, 2002370.
[31] Nezhad-Mokhtari, P.; Ghorbani, M.; Abdyazdani, N. Reinforcement of hydrogel scaffold using oxidized-guar gum incorporated with curcumin-loaded zein nanoparticles to improve biological performance. *Int. J. Biol. Macromol.* **2021**, *167*, 59–65.
[32] Du, X. C.; Wu, L.; Yan, H. Y.; Jiang, Z. Y.; Li, S. L.; Li, W.; Bai, Y. L.; Wang, H. J.; Cheng, Z. J.; Kong, D. L. et al. Microchannelled alkylated chitosan sponge to treat noncompressible hemorrhages and facilitate wound healing. *Nat. Commun.* **2021**, *12*, 4733.
[33] Pandit, A. H.; Nisar, S.; Imtiyaz, K.; Nadeem, M.; Mazumdar, N.; Rizvi, M. M. A.; Ahmad, S. Injectable, self-healing, and biocompatible N, O-carboxymethyl chitosan/multialdehyde guar gum hydrogels for sustained anticancer drug delivery. *Biomacromolecules* **2021**, *22*, 3731–3745.
[34] Poustchi, F.; Amani, H.; Ahmadian, Z.; Niknezhad, S. V.; Mehrabi, S.; Santos, H. A.; Shahbazi, M. A. Combination therapy of killing diseases by injectable hydrogels: From concept to medical applications. *Adv. Healthcare Mater.* **2021**, *10*, 2001571.
[35] Li, Y. L.; Rodrigues, J.; Tomás, H. Injectable and biodegradable hydrogels: Gelation, biodegradation and biomedical applications. *Chem. Soc. Rev.* **2012**, *41*, 2193–2221.
[36] Cushing, M. C.; Anseth, K. S. Hydrogel cell cultures. *Science* **2007**, *316*, 1133–1134.
[37] Hoffman, A. S. Hydrogels for biomedical applications. *Adv. Drug Deliv. Rev.* **2012**, *64*, 18–23.
[38] Mao, X. Y.; Cheng, R. Y.; Zhang, H. B.; Bae, J.; Cheng, L. Y.; Zhang, L.; Deng, L. F.; Cui, W. G.; Zhang, Y. G.; Santos, H. A. et al. Self-healing and injectable hydrogel for matching skin flap regeneration. *Adv. Sci.* **2019**, *6*, 1801555.
[39] Qu, J.; Zhao, X.; Liang, Y. P.; Zhang, T. L.; Ma, P. X.; Guo, B. L. Antibacterial adhesive injectable hydrogels with rapid self-healing, extensibility and compressibility as wound dressing for joints skin wound healing. *Biomaterials* **2018**, *183*, 185–199.
[40] Zhu, H. F.; Kong, B.; Nie, M.; Zhao, C.; Liu, R.; Xie, Y.; Zhao, Y. J.; Sun, L. Y. ECM-inspired peptide dendrimer microgels with human MSCs encapsulation for systemic lupus erythematosus treatment. *Nano Today* **2022**, *43*, 101454.
[41] Liu, R.; Kong, B.; Chen, Y.; Liu, X. P.; Mi, S. L. Formation of helical alginate microfibers using different G/M ratios of sodium alginate based on microfluidics. *Sens. Actuators B:Chem.* **2020**, *304*, 127069.